SIMS Iron Isotope Measurements of the Balmat Pyrite Reference Material: A Non-Unique δ^{56}Fe Signature

Virgil **Pasquier** (1)* (iD), Eric S. **Rego** (2), Juliette **Dupeyron** (1,3), Anne-Sophie **Bouvier** (1) (iD), Thomas **Bovay** (1), Martin **Robyr** (1) and Johanna **Marin-Carbonne** (1)

(1) Institut des Sciences de la Terre, Université de Lausanne, Switzerland
(2) Origins Laboratory, Department of Geophysical Sciences, The University of Chicago, USA
(3) Université Paris Cité, Institut de Physique du Globe, CNRS, Paris F-75005, France
* Corresponding author. e-mail: virgil.pasquier@unil.ch

In situ iron isotope ratios (δ^{56}Fe) in sulfide measured by secondary ion mass spectrometry (SIMS) can provide valuable information on several of Earth's surface processes. SIMS relies on the use of a matrix-matched reference material to correct for instrumental mass fractionation. To date Balmat pyrite has been widely used as a reference material, on the assumption of its homogeneous δ^{56}Fe composition. However, several studies have reported divergent bulk δ^{56}Fe values, which may jeopardise its use. Here, we combined bulk solution MC-ICP-MS and *in situ* SIMS δ^{56}Fe measurements on two Balmat batches: the Balmat-Original published in Whitehouse and Fedo (2007) and Balmat-UNIL. Despite similar compositions, this study demonstrates the existence of two isotopically distinct Balmat populations. With respect to Balmat-Original (δ^{56}Fe = -0.39 $\pm$ 0.05‰, 2s), Balmat-UNIL is isotopically 'lighter' with a bulk solution MC-ICP-MS composition of -1.46 $\pm$ 0.024‰. Additionally, Balmat-UNIL has two subpopulations: the first is characterised by δ^{56}Fe values of -1.46 $\pm$ 0.25‰, whereas the second agrees with the original Balmat batch. In each Balmat-UNIL subpopulation, the intra-grain and inter-grain variabilities are sufficient to use Balmat as a reference material for δ^{56}Fe isotope measurements by SIMS. This study revealed at least two end-member compositions of Balmat pyrite and calls for a careful batch-specific determination of bulk δ^{56}Fe.

Keywords: iron isotopes, matrix-matched reference material, secondary ion mass spectrometry, pyrite, Balmat, Ruttan.

Iron (Fe) is the fourth most abundant element in Earth's upper crust (Rudnick and Gao 2003), a key nutrient for life, and a redox-sensitive element (e.g., Fitzsimmons and Conway 2023). In addition, recent studies have suggested that the redox cycling between Fe(II) and Fe(III) played a fundamental role in the early Earth's environmental biogeochemistry (e.g., Kappler *et al.* 2021). Consequently, over the last two decades, Fe stable isotope geochemistry has developed rapidly to investigate what controls the global oceanic Fe cycle, sources, internal cycling, and microbial fractionations (e.g., Fitzsimmons and Conway 2023, Weber and Deutsch 2010).

Redox cycling affects the Fe isotopic fractionation of the four Fe isotopes, ^{54}Fe (5.80%), ^{56}Fe (91.72%), ^{57}Fe (2.20%) and ^{58}Fe (0.28%), following mass- and temperature-dependent fractionation laws (e.g., Dauphas

and Schauble 2016, Dauphas *et al.* 2017). The Fe isotopic composition is usually reported using the delta notation (δ^{56}Fe), which is defined as the deviation in part of permil of the ^{56}Fe/^{54}Fe ratio relative to the international reference value from IRMM-014 (Craddock and Dauphas 2011). Traditionally, δ^{56}Fe are measured as bulk solution using multi-collector inductively coupled plasma-mass spectrometry (MC-ICP-MS) with an analytical precision (2s) around $\pm$0.05‰ or lower (Dauphas *et al.* 2017, Heard and Dauphas 2020). However, *in situ* δ^{56}Fe measurements by secondary ion mass spectrometry (SIMS) and/or laser ablation coupled to a multi-collector inductively coupled plasma-mass spectrometer (LA-MC-ICP-MS) are becoming more common for samples displaying large isotopic fractionation such as observed in pyrite, where the typical SIMS analytical precision for

GEOSTANDARDS and GEOANALYTICAL *RESEARCH*

Table 1.
Solution MC-ICP-MS and microscale Fe isotopic δ^{56}Fe and δ^{57}Fe values of the various published batches of Balmat pyrite

δ^{56}Fe (‰)	2s	δ^{57}Fe (‰)	2s	n	Method	Reference
-0.39	0.05				MC-ICP-MS	Whitehouse and Fedo (2007)
-1.38	0.07	-2.01	0.11	31	MC-ICP-MS	Zheng *et al.* (2018)
-1.33	0.05	-1.96	0.11	4	MC-ICP-MS	Xie *et al.* (2018)
-1.30	0.04	-1.94	0.04	3	SN-MC-ICP-MS	Xu *et al.* (2022)
-1.32	0.16	-1.93	0.25	166	fs LA-MC-ICP-MS	Xu *et al.* (2022)
-1.46	**0.02**	**-2.15**	**0.03**	**9**	**MC-ICP-MS**	**This study**

pyrite is around 0.20‰ (2s, Decraene *et al.* 2021a). Indeed, over Earth's history the overall pyrite bulk δ^{56}Fe variability ranges between -4 and +1‰, allowing SIMS δ^{56}Fe investigation at the pyrite population level (e.g., Decraene *et al.* 2021b, Harazim *et al.* 2020, Whitehouse and Fedo 2007) and/or internal grain scale (e.g., Marin-Carbonne *et al.* 2014). Interestingly, Dupeyron *et al.* (2023) compiled available microscale δ^{56}Fe and found an overall wider isotopic variability, i.e., -4 to +4‰, preserved in Precambrian sedimentary rocks opening a new avenue for *in situ* Fe isotope investigation.

Accurate microscale δ^{56}Fe determination by SIMS relies on the ability to correct for the instrumental mass fractionation (IMF) and, therefore, on the use of adequate matrix-matched reference materials. In a pioneering study, Whitehouse and Fedo (2007) evaluated the IMF and measurement reproducibility of δ^{56}Fe in pyrite using one of the commonly used sulfur isotope reference materials: Balmat (Crowe and Vaughan 1996). Their MC-ICP-MS data ($n = 2$) yield a δ^{56}Fe value of -0.39 ± 0.05‰ (2s), which was subsequently applied to investigate intra-grain homogeneity by SIMS using three grains of the same Balmat batch (hereafter referred to as Balmat-ORIGINAL). After intra- and inter-grain homogeneity investigation, they concluded that Balmat-ORIGINAL was sufficiently homogenous to be used as a SIMS Fe isotope reference material, with a δ^{56}Fe = -0.39 ± 0.18‰ (2s). Since that study, the following determination of pyrite δ^{56}Fe values by SIMS has used the δ^{56}Fe value of Balmat-ORIGINAL for correction of the IMF and/or accuracy calculation (e.g., Decraene *et al.* 2021b, Marin-Carbonne *et al.* 2011). It is worth noting that all these previous studies have tested the suitability of the Balmat reference material by using secondary pyrite reference materials, which have all given good agreement between SIMS measurements and MC-ICP-MS values. Yet, more recent solution MC-ICP-MS analyses, carried out on different Balmat batches (i.e., same sampling locality but different sampling aliquot), have reported δ^{56}Fe deviations from the initial δ^{56}Fe values (i.e., a δ^{56}Fe = -0.39), see Table 1.

However, with the increasing number of pyrite microscale δ^{56}Fe determinations, The community must investigate the relative isotopic homogeneity of the Balmat deposit. Therefore, this study presents the first systematic comparison of bulk solution MC-ICP-MS and *in situ* SIMS δ^{56}Fe measurements from two distinct Balmat batches: the ORIGINAL *vs.* our in-house aliquot (Balmat-UNIL). In addition, we investigated a potential new reference material for Fe isotope determination in pyrite: Ruttan-UNIL.

Experimental

Balmat pyrite batches

In this study, we used two different pyrite aliquots of the Balmat deposit: Balmat-ORIGINAL and Balmat-UNIL. For Balmat-ORIGINAL, two large grains (courtesy of M. Whitehouse) were embedded in epoxy and polished with diamond pastes to ensure a flat surface prior to being carefully removed from the epoxy and pressed into a 1-inch indium mount, hereafter referred to as MM-1 (red symbols in Figures 1 and 2). The bulk solution MC-ICP-MS δ^{56}Fe value of Balmat-ORIGINAL is taken from Whitehouse and Fedo (2007) to be equal to δ^{56}Fe = -0.39 ± 0.18‰ (2s). One of these grains was the pyrite reference material used in the studies of Marin-Carbonne *et al.* (2011) and Decraene *et al.* (2021).

The same procedure was applied to the Balmat-UNIL batch, yielding an indium mount with two Balmat-UNIL grains, hereafter referred to as MM-2 (blue symbols in Figures 1 and 2). To determine the δ^{56}Fe values for the Balmat-UNIL, nine fragments were randomly selected, examined under optical microscopy to ensure the absence of any other Fe-bearing minerals phases (e.g., sphalerite, pyrrhotite, chalcopyrite), and characterised by bulk solution MC-ICP-MS at the University of Chicago.
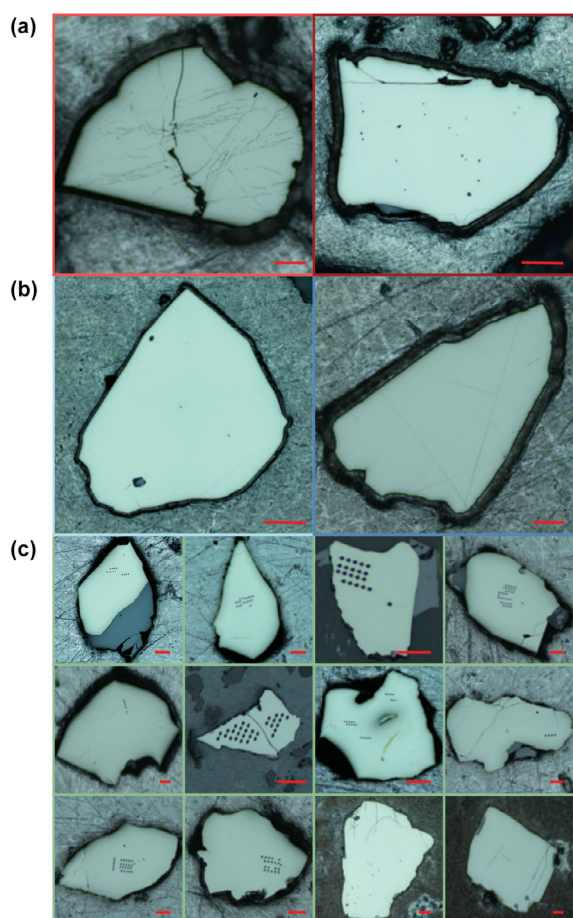
Figure 1. Grain morphologies as revealed by optical microscopy imaging of (a) Balmat-ORIGINAL grains in MM1, (b) Balmat-UNIL in MM2 and (c) representative Balmat grains in "sample mounts". Red scale bars are 100 μm long.

In addition, sixteen individual polished Balmat-UNIL grains were mounted in sixteen different indium mounts, hereafter referred to as 'sample mounts' (green symbols in Figure 1).

Ruttan pyrite

Similarly, six Ruttan-UNIL pyrite fragments (courtesy of D.E. Crowe) were randomly handpicked, examined for other Fe-bearing phases under an optical microscope and, then, similarly characterised by bulk solution MC-ICP-MS at the University of Chicago.

As previously, sixteen individual Ruttan-UNIL polished grains were pressed into sixteen indium mounts alongside the Balmat-UNIL 'sample', hereafter also referred to as 'sample mounts' (green symbols in Figure 1).

Chemical characterisation of the pyrite material

The chemical composition of the pyrite grains was measured using an electron probe microanalyser (EPMA) at the Centre of Advanced Surface Analyses of the University of Lausanne (CASA). EPMA transects were performed using the five-spectrometer equipped JEOL JXA 8530F. The analytical conditions were the following: a fully focused beam (with a diameter of less than 1 μm) of 15 nA beam current and an acceleration potential of 15 kV. A set of sulfide, silicate, and oxides was used as reference material.

Elements and X-ray lines used for analysis were Fe ($K\alpha$), Co ($K\alpha$), Ni ($K\alpha$), Cu ($K\alpha$), Zn ($K\alpha$), S ($K\alpha$), Mn ($K\alpha$) and Pb ($M\alpha$). Detection limits were below 144 μg g^{-1} for Co, 167 μg g^{-1} for Cu, 120 μg g^{-1} for Mn, 654 μg g^{-1} for Pb, 145 μg g^{-1} for Cr, and 200 μg g^{-1} for Zn on average.

Solution MC-ICP-MS

The analytical procedure used for Fe purification and isotopic measurements followed the standard procedures used at the Origins Laboratory of the University of Chicago (e.g., Dauphas et al. 2009, Hopp et al. 2022).

Briefly, hand-picked pyrite grains were digested using HF-HNO$_3$ (2:1) at 130 °C on a hot plate for 48 h followed by several steps of aqua regia (3:1 HCl-HNO$_3$) dissolution, later converted and re-dissolved in 0.25 ml of 10 mol l^{-1} HCl for column purification. We used 10.5 cm long PFA columns (0.62 cm inner diameter) filled with 3 ml pre-cleaned AG1-X8 (200–400 mesh) anion resin to efficiently separate Fe from Cu, Ni, Co and Cr as described by Tang and Dauphas (2012). Nickel and major elements were eluted in 5 ml 10 mol l^{-1} HCl, while Cu and other contaminants were eluted using 30 ml 4 mol l^{-1} HCl. Iron was finally collected in 9 ml 0.4 mol l^{-1} HCl. The entire procedure was repeated twice for each sample.

Iron isotopic measurements were performed at the University of Chicago using a Thermo Scientific Neptune MC-ICP-MS. Measurements were made on flat-topped peak shoulder in high-resolution mode. All isotopes were measured using 10^{11} Ω amplifiers except for ^{56}Fe$^+$, which was measured using a 10^{10} Ω amplifier. We monitored possible isobaric interferences by measuring simultaneously ^{53}Cr$^+$ and ^{60}Ni$^+$ using 10^{12} Ω amplifiers. Platinum cones were used to increase sensitivity (Hopp et al. 2022). The purified Fe solutions (5 μg g^{-1} in 0.3 mol l^{-1} HNO$_3$) were introduced into the MC-ICP-MS using a cyclonic spray
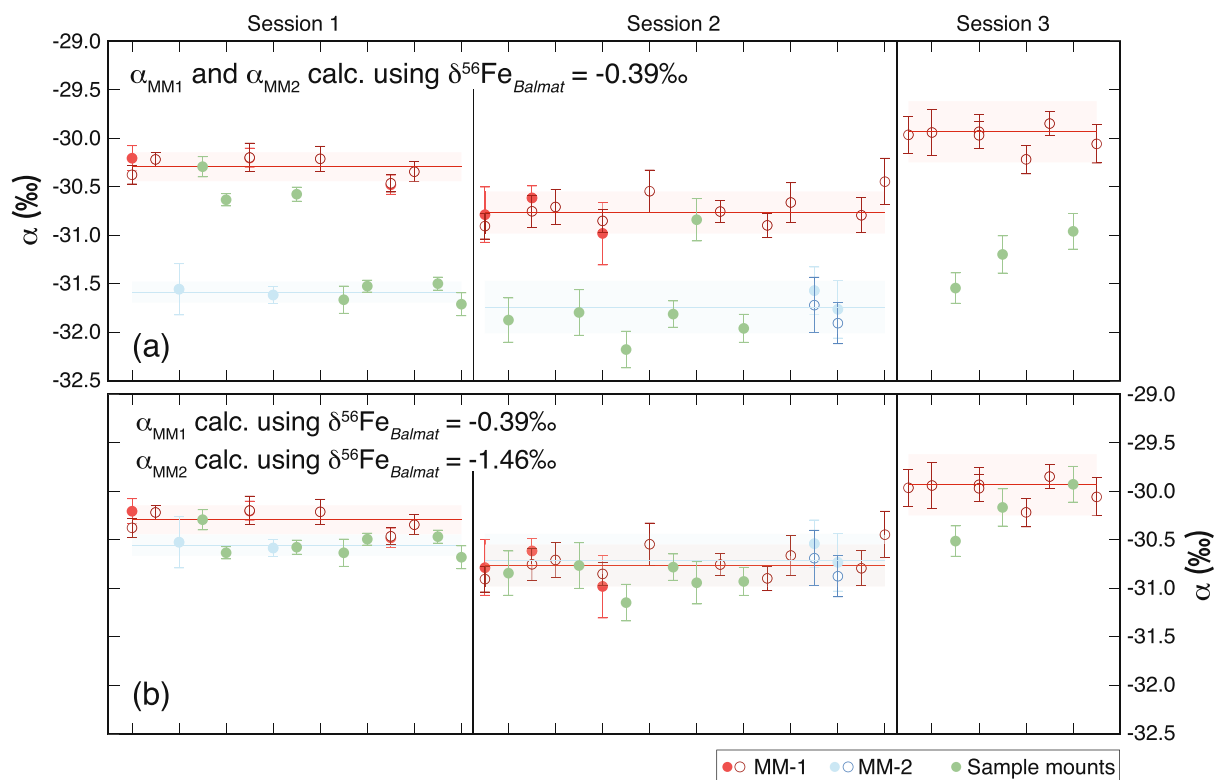
Figure 2. Instrumental Mass Fractionation (α). In panel (a), α_{MM1} and α_{MM2} calculated using the solution MC-ICP-MS from the Balmat-ORIGINAL batch (Whitehouse and Fedo 2007); In panel (b), α_{MM1} and α_{MM1} calculated with MC-ICP-MS values from Balmat-ORIGINAL (Whitehouse and Fedo 2007) and Balmat-UNIL (this study), respectively. Red symbols refer to MM1 (only Balmat-ORIGINAL), Blue symbols refer to MM2 (only Balmat-UNIL) and green symbols refer to 'Sample Mounts'. Open and filled symbols show the two Balmat fragments, as mentioned in the section *Balmat pyrite batches*. Coloured horizontal lines and associated shaded areas correspond to the long-term mean values and associated uncertainties (2s). Vertical black lines show session boundaries.

chamber. Standard-sample bracketing was used to correct Fe isotopic ratio measurements for instrumental mass fractionation. The mass fractions of the samples and reference materials were matched to ≤ 2%. Iron isotopic ratios are reported in the usual δ notation in per mil (‰) as:

$$\delta^{56}Fe = \left[\left({}^{56}Fe/{}^{54}Fe \right)_{sample} / \left({}^{56}Fe/{}^{54}Fe \right)_{standard} - 1 \right] \quad (1)$$

where the "standard" is IRMM-524a which has identical isotopic composition to IRMM-14 (Craddock and Dauphas 2011). The uncertainties are reported as 2s.

SIMS iron isotope measurements

Prior to SIMS $\delta^{56}Fe$ investigation, all mounts were subjected to an optical profiler (Contour GT-K, Bruker, Karlsruhe, Germany) at the University of Lausanne to guarantee minimal topography (< 5 μm, Kita *et al.* 2009)

and coated with a 35 nm gold film to ensure conductivity between the sample surface and the SIMS holder.

All microscale investigations were carried out at the University of Lausanne using the SwissSIMS Cameca 1280-HR ion probe equipped with a Hyperion-II radio-frequency source. We undertook three measurement sessions: the first between 03/05/2023 and 07/05/2023, the second between 09/05/2023 and 12/05/2023, and the third between 20/06/2023 and 23/06/2023. Note that the Hyperion source was turned off and the primary beam was re-focused between session 1 and session 2. Maximal measurement repeatability ("internal") precision (2SE) was 0.18, 0.21 and 0.14 for sessions 1, 2 and 3, respectively.

The ion microprobe settings for this study were the same as those used by Decraene *et al.* (2021a). The key instrumental parameters are summarised below, but details can be found in Decraene *et al.* (2021a). A 3 nA Gaussian $^{16}O^-$ beam was

focused to a spot diameter of ≈ 3 μm on the sample surface. Secondary Fe ions were measured in the mass spectrometer with typical ^{56}Fe intensities between 5 to 6×10^7 counts per second. To resolve the ^{53}CrH$^+$ (on the ^{54}Fe$^+$) and ^{55}MnH$^+$ (on the ^{56}Fe$^+$) the mass resolution power was set to ≈ 6800, and the measurement of ^{52}Cr allowed to monitor the ^{54}Cr$^+$ isobaric interference on the ^{54}Fe$^+$ (Whitehouse and Fedo 2007, Marin-Carbonne et al. 2011). ^{52}Cr, ^{54}Fe and ^{56}Fe were simultaneously measured in multi-collection mode with two off-axis Faraday cups and one electron multiplier for ^{52}Cr. A 90 s pre-sputtering time was applied before each analysis, allowing simultaneous detector background acquisition. Data acquisition was performed as sixty cycles for a total of 7 min per analysis resulting in a ~ 3 μm deep pit. After the pre-sputtering, (i) beam centring in the field and contrast apertures and (ii) sample high voltage scanning to monitor possible energy offset were performed automatically before each data collection.

The data reduction procedure used in this study is adapted from Farquhar et al. (2013). First, each detector was corrected for its gain and background, and then the detector yields were ^{54}Cr$^+$ corrected using:

$$^{54}\text{Fe}_{corr}\ cps = \ ^{54}\text{Fe}\ cps - \left[^{52}\text{Cr}\ cps \times \left(^{54}\text{Cr}/^{52}\text{Cr}\right)\right] \quad (2)$$

$$\delta^{56}\text{Fe}_{corr} = 1000 \times \left[\left(\left(56\text{Fe}\ cps/\ ^{54}\text{Fe}_{corr}\ cps\right)/\right.\right.$$
$$\left.\left.\left(^{56}\text{Fe}_{IRMM-014}/^{54}\text{Fe}_{IRMM-014}\right)\right) - 1\right] \quad (3)$$

where cps refers to counts per second and ^{56}Fe$_{IRMM-014}/^{54}$Fe$_{IRMM-014}$ equals 15.6979 (Craddock and Dauphas 2011).

After the drift correction, the IMF (α) was calculated as the weighted mean of our internal bracketing standard measured every ten to fifteen analyses (e.g., Balmat-ORIGINAL and/or Balmat-UNIL) using:

$$\alpha = \left[1 + \left(\delta^{56}\text{Fe}_{corr}/1000\right)\right]/\left[1 + \left(\delta^{56}\text{Fe}_{std}/1000\right)\right] \quad (4)$$

where δ^{56}Fe$_{std}$ is the solution MC-ICP-MS values relative to IRMM-014 (^{56}Fe/^{54}Fe = 15.6979, Craddock and

Dauphas 2011). The δ^{56}Fe$_{sample}$ was then calculated using:

$$\delta^{56}\text{Fe}_{sample} = 1000 \times \left[\left(1 + \left(\delta^{56}\text{Fe}_{corr}/1000\right)/\alpha\right) - 1\right] \quad (5)$$

The total error is reported as 2s and is a combination of the two independent parameters: (a) the "internal error" inherent to the counting statistics for each measurement, and (b) the error on the primary reference material associated with the averaged bulk solution values. Our statistical treatment of error propagation uses the standard deviations to calculate the resulting uncertainty.

Results and discussion

Chemical analyses of pyrites

The major Fe and S elemental mass fractions of Balmat-ORIGINAL and Balmat-UNIL were consistent with each other and with previously published data (Table 2). The trace element contents of the pyrite were below the detection limit for all the elements determined (i.e., Co, Ni, Mn, Cr, Zn, Cu and Pb).

Solution MC-ICP-MS

The mean Fe isotope delta values of the nine Balmat-UNIL grains measured in solution MC-ICP-MS were δ^{56}Fe = -1.46 ± 0.02‰ and δ^{57}Fe = -2.15 ± 0.03‰ (Table 1). As such, the Balmat-UNIL is 1.07 ± 0.01‰ isotopically 'lighter' than the Balmat-ORIGINAL The six Ruttan-UNIL bulk solution MC-ICP-MS δ^{56}Fe and δ^{57}Fe values were averaged at -1.00 ± 0.02‰ and -1.48 ± 0.03‰.

SIMS Balmat IMF

In the following paragraph, all IMF values (α) are described as the difference between the SIMS raw values

Table 2.
Pyrite iron and sulfur mass fractions (in % m/m)

Name	Fe (% m/m)	2s	S (% m/m)	2s	Reference
Balmat-ORIGINAL	46.50		53.60		Marin Carbonne et al. (2011)
Ruttan-ORIGINAL	44.54		52.41		Crowe and Vaughan (1996)
Balmat-UNIL	46.28	0.30	53.93	0.58	This study
Ruttan-UNIL	46.25	0.23	54.04	0.41	This study

and the solution MC-ICP-MS δ^{56}Fe from the Balmat-ORIGINAL, as reported in Whitehouse and Fedo (2007) (i.e., δ^{56}Fe = -0.39 $\pm$ 0.05‰) (see Figure 2a). During the first session, the mean α values were -30.29 $\pm$ 0.30‰ and -31.58 $\pm$ 0.22‰, for MM1 and MM2 respectively. The isotopic offset between MM1 and MM2 is 1.29 $\pm$ 0.37‰. Sample mounts α values range between -30.29 $\pm$ 0.20‰ and -31.71 $\pm$ 0.24‰, and appear to follow a bimodal distribution centred around the mean α values of MM1 and/or MM2 (Figure 2a).

This dichotomy in α values between MM1 and MM2 was also observed in the second session, where α_{MM1} = -30.76 $\pm$ 0.43‰ and α_{MM2} = -31.74 $\pm$ 0.54‰, creating an isotopic offset of +0.97 $\pm$ 0.69‰. Similarly, sample mounts appear to have a bi-modal distribution around MM1 and MM2 mean α values, yet the lower mode (i.e., as in MM2) is more frequent (Figure 2a).

During the third session, only MM1 has been analysed and presents an α value of -29.93 $\pm$ 0.63‰. Samples mounts analysed during the third session show a mean α value of -31.24 $\pm$ 0.58‰. The mean offset between MM1 and sample mounts is +1.31 $\pm$ 0.86‰ (Figure 2a).

Please note that relative to session 1, the two subsequent measurement sessions (i.e., session 2 and session 3) showed a low "external precision" on δ^{56}Fe due to a source aging, resulting in a less stable primary intensity.

We note that the isotopic offset between MM1 and MM2, and more generally between the two α modes is statistically indistinguishable from the isotopic offset measured by solution MC-ICP-MS between the two Balmat batches (i.e., Balmat-ORIGINAL vs. Balmat-UNIL). Moreover, we calculated the α_{MM2} values using the solution MC-ICP-MS δ^{56}Fe of Balmat-UNIL, and the isotopic differences between MM1 and MM2 was drastically reduced, and now, statistically indistinguishable (see Figure 1b). The α_{MM1} and α_{MM2} are -30.29 $\pm$ 0.30‰ and -30.55 $\pm$ 0.21‰ during the first session, and -30.76 $\pm$ 0.63‰ and -30.71 $\pm$ 0.54‰ throughout the second session. The isotopic offset between MM1 and MM2 ($\Delta_{\alpha MM1-\alpha MM2}$) is +0.26 $\pm$ 0.37‰ and +0.05 $\pm$ 0.83‰ for sessions 1 and 2 respectively.

The same procedure was applied to the sample mounts characterised by α values isotopically lighter than MM1 (all except four sample mounts), resulting in α_{sample} values statistically indistinguishable from the session mean α_{MM1} and/or α_{MM2}. If considering the four exceptions mentioned above, indistinguishable α values were obtained by applying the original solution MC-ICP-MS δ^{56}Fe (i.e., δ^{56}Fe = -0.39 $\pm$ 0.05‰, Whitehouse and Fedo 2007) (Figure 2b).

Based on our measurements (bulk solution MC-ICP-MS and *in situ* SIMS), it is evident that different Balmat batches (e.g., Balmat-ORIGINAL and/or Balmat-UNIL) share the same petrological (Figure 1) and bulk chemistry (Table 2) characteristics, yet they may have different δ^{56}Fe bulk isotopic compositions. In addition, we note that the Balmat-UNIL batch preserved at least two populations of pyrite grain that are isotopically distinct in δ^{56}Fe values (i.e., where Balmat-UNIL is 1.07 $\pm$ 0.01‰ isotopically 'lighter' than the Balmat-ORIGINAL). From our literature survey (Table 1), it appears that those two populations are not a characteristic of our in-house Balmat-UNIL batch, but may also be present in other in-house batches as the bulk iron isotopic composition of Balmat-UNIL is in agreement within uncertainties with other measurements (Zheng *et al.* 2018, Xu *et al.* 2022).

Nevertheless, as in Whitehouse and Fedo (2007), the intra-grain and inter-grain variation in each sub-population appears to be sufficiently homogeneous to use Balmat as a SIMS reference material for Fe isotope measurement in pyrite. Yet, we encourage the community to carry out homogeneity tests on their in-house Balmat sub-population to be confident in the δ^{56}Fe values to use for IMF correction, and to report new Balmat batches relative to 'Balmat-Original' as reported in Whitehouse and Fedo (2007).

SIMS Ruttan δ^{56}Fe

The δ^{56}Fe values for SIMS Ruttan, as detailed in the subsequent paragraph, have been derived from the δ^{56}Fe values acquired through solution MC-ICP-MS analysis allowing similar α values in MM1, MM2 and sample mounts (Figure 3). Ruttan fragments included in MM1 and in the four 'exception' samples were calculated using the α values of the Balmat-ORIGINAL, whereas Ruttan fragments embedded in MM2 and the sample mounts (except the four previously mentioned) were calculated using the Balmat-UNIL solution MC-ICP-MS δ^{56}Fe values.

The δ^{56}Fe values measured by SIMS range from -1.82 $\pm$ 0.36‰ to +0.84 $\pm$ 0.08‰, the mean δ^{56}Fe values are -0.12 $\pm$ 0.53‰, -0.22 $\pm$ 1.32‰ and -0.08 $\pm$ 0.52‰ for the first, second and third sessions, respectively (Figure 3). From the twenty Ruttan fragments tested in this study, only a unique grain appears to yield a consistent δ^{56}Fe with the solution MC-ICP-MS (Figure 3). This observation is consistent with the

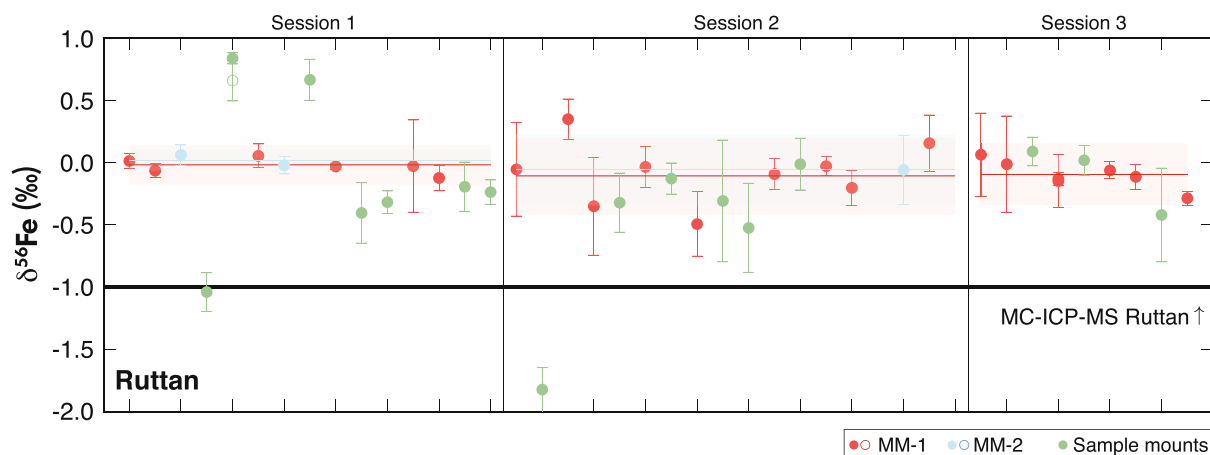**Figure 3.** Calculated Ruttan δ^{56}Fe using α values from Figure 1b. The horizontal thick line shows the solution MC-ICP-MS δ^{56}Fe measured in Ruttan. Symbols are the same as in Figure 2.

wide inter-grain variation in δ^{56}Fe of > 1.12‰ (while being internally relatively homogeneous, i.e., ranging from 0.05 to 0.49‰ with a mean precision of ± 0.36‰ (2s) over the three measurement sessions). Consequently, from our investigation, Ruttan is clearly inappropriate as a SIMS reference material for Fe isotopes in pyrite.

Conclusions

The number of microscale δ^{56}Fe analyses in pyrite, measured either by SIMS and/or LA-MC-ICP-MS, has increased drastically over the last 10 years (Agangi et al. 2015, Czaja et al. 2018, Decraene et al. 2021a, Decraene et al. 2021b, Dupeyron et al. 2023, Galić et al. 2017, Harazim et al. 2020, Liu et al. 2022, Marin-Carbonne et al. 2020, Marin-Carbonne et al. 2014, Nishizawa et al. 2010, Virtasalo et al. 2015, Virtasalo et al. 2013, Xing et al. 2022, Yoshiya et al. 2012, Yoshiya et al. 2015a, Yoshiya et al. 2015b, Zhang et al. 2022a, Zhang et al. 2022b, Zheng et al. 2018). The pioneering work of Whitehouse and Fedo (2007) developed and proposed to use natural pyrite originating from the Balmat deposit (Adirondack Mountains, New York) as a Fe reference material for SIMS measurements. Indeed, their investigations revealed a minimal intra- and inter-grain variability converging toward δ^{56}Fe values of -0.39 $\pm$ 0.18‰ (referred to in this study as Balmat-ORIGINAL). Subsequent studies have used this value to correct for IMF, yet, to date, no homogeneity tests have been carried out on different Balmat batches, i.e., same locality but different sub-sampling.

Here, we used bulk solution MC-ICP-MS and *in situ* SIMS techniques to investigate the δ^{56}Fe preserved in our in-house

Balmat batch, called Balmat-UNIL. Our work revealed that Balmat-UNIL preserved at least two pyrite populations, both of which have similar petrological and chemical characteristics but distinct δ^{56}Fe values. The first population in Balmat-UNIL is characterised by δ^{56}Fe values of -1.46 $\pm$ 0.25‰, whereas the second population has a δ^{56}Fe consistent with the original Balmat batch. Importantly, the intra-grain and inter-grain isotopic variability in each sub-population appears to be sufficiently homogeneous to use Balmat as a SIMS reference material for Fe isotope in pyrite. Yet, accurate IMF corrections require knowing the exact solution MC-ICP-MS δ^{56}Fe values of both populations. Importantly, our literature survey revealed that other isotopically distinct Balmat populations might exist. To overcome this issue, we have investigated the potential of Ruttan pyrite, a commonly used sulfur isotope reference material. While being internally homogeneous, our results show a wide inter-grain variability, with up to 1.12‰ variation ($n = 20$), which makes Ruttan a poor candidate as a SIMS Fe isotope reference material. Finally, we hope that this assessment will spur action toward a community effort to develop a better microscale Fe reference material.

Acknowledgements

Scientific editing by Paul J. Sylvester. Open access funding provided by Universite de Lausanne.

Data availability statement

All data needed to evaluate the conclusions in the paper may be requested from the authors.

References

Agangi A., Hofmann A., Rollion-Bard C., Marin-Carbonne J., Cavalazzi B., Large R. and Meffre S. (2015)
Gold accumulation in the Archaean Witwatersrand Basin, South Africa – Evidence from concentrically laminated pyrite. Earth-Science Reviews, 140, 27–53.

Craddock P.R. and Dauphas N. (2011)
Iron isotopic compositions of geological reference materials and chondrites. Geostandards and Geoanalytical Research, 35, 101–123.

Crowe D.E. and Vaughan R.G. (1996)
Characterization and use of isotopically homogeneous standards for in situ laser microprobe analysis of $^{34}S/^{32}S$ ratios. American Mineralogist, 81, 187–193.

Czaja A.D., Van Kranendonk M.J., Beard B.L. and Johnson C.M. (2018)
A multistage origin for Neoarchean layered hematite-magnetite iron formation from the Weld Range, Yilgarn Craton, Western Australia. Chemical Geology, 488, 125–137.

Dauphas N., John S.G. and Rouxel O. (2017)
Iron isotope systematics. Non-Traditional Stable Isotopes, 82, 415–510.

Dauphas N., Pourmand A. and Teng F.-Z. (2009)
Routine isotopic analysis of iron by HR-MC-ICP-MS: How precise and how accurate? Chemical Geology, 267, 175–184.

Dauphas N. and Schauble E.A. (2016)
Mass fractionation laws, mass-independent effects, and isotopic anomalies. Annual Review of Earth and Planetary Sciences, 44, 709–783.

Decraene M.N., Marin-Carbonne J., Bouvier A.S., Villeneuve J., Bouden N., Luais B. and Deloule E. (2021a)
High-spatial-resolution measurements of iron isotopes in pyrites by secondary ion mass spectrometry using the new Hyperion-II radio-frequency plasma source. Rapid Communications in Mass Spectrometry, 35, e8986.

Decraene M.N., Marin-Carbonne J., Thomazo C., Olivier N., Philippot P., Strauss H. and Deloule E. (2021b)
Intense biogeochemical iron cycling revealed in Neoarchean micropyrites from stromatolites. Geochimica et Cosmochimica Acta, 312, 299–320.

Dupeyron J., Decraene M.-N., Marin-Carbonne J. and Busigny V. (2023)
Formation pathways of Precambrian sedimentary pyrite: Insights from in situ Fe isotopes. Earth and Planetary Science Letters, 609, 118070.

Farquhar J., Cliff J., Zerkle A.L., Kamyshny A., Poulton S.W., Claire M., Adams D. and Harms B. (2013)
Pathways for Neoarchean pyrite formation constrained by mass-independent sulfur isotopes. Proceedings of the National Academy of Sciences of the USA, 110, 17638–17643.

Fitzsimmons J.N. and Conway T.M. (2023)
Novel insights into marine iron biogeochemistry from iron isotopes. Annual Review of Marine Science, 15, 383–406.

Galić A., Mason P.R.D., Mogollón J.M., Wolthers M., Vroon P.Z. and Whitehouse M.J. (2017)
Pyrite in a sulfate-poor Paleoarchean basin was derived predominantly from elemental sulfur: Evidence from 3.2 Ga sediments in the Barberton Greenstone Belt, Kaapvaal Craton. Chemical Geology, 449, 135–146.

Harazim D., Virtasalo J.J., Denommee K.C., Thiemeyer N., Lahaye Y. and Whitehouse M.J. (2020)
Exceptional sulfur and iron isotope enrichment in millimetre-sized, early Palaeozoic animal burrows. Scientific Reports, 10, 20270.

Heard A.W. and Dauphas N. (2020)
Constraints on the coevolution of oxic and sulfidic ocean iron sinks from Archean-Paleoproterozoic iron isotope records. Geology, 48, 358–362.

Hopp T., Dauphas N., Spitzer F., Burkhardt C. and Kleine T. (2022)
Earth's accretion inferred from iron isotopic anomalies of supernova nuclear statistical equilibrium origin. Earth and Planetary Science Letters, 577, 117245.

Kappler A., Bryce C., Mansor M., Lueder U., Byrne J.M. and Swanner E.D. (2021)
An evolving view on biogeochemical cycling of iron. Nature Reviews, Microbiology, 19, 360–374.

Kita N.T., Ushikubo T., Fu B. and Valley J.W. (2009)
High precision SIMS oxygen isotope analysis and the effect of sample topography. Chemical Geology, 264, 43–57.

Liu Y.R., Ding W.M., Lang X.G., Xing C.C., Wang R.M., Huang K.J., Fu B., Ma H.R., Peng Y.B. and Shen B. (2022)
Refining the early Cambrian marine redox profile by using pyrite sulfur and iron isotopes. Global and Planetary Change, 213, 103817.

Marin-Carbonne J., Busigny V., Miot J., Rollion-Bard C., Muller E., Drabon N., Jacob D., Pont S., Robyr M., Bontognali T.R.R., Francois C., Reynaud S., Van Zuilen M. and Philippot P. (2020)
In Situ Fe and S isotope analyses in pyrite from the 3.2 Ga Mendon Formation (Barberton Greenstone Belt, South Africa): Evidence for early microbial iron reduction. Geobiology, 18, 306–325.

Marin-Carbonne J., Rollion-Bard C., Bekker A., Rouxel O., Agangi A., Cavalazzi B., Wohlgemuth-Ueberwasser C.C., Hofmann A. and McKeegan K.D. (2014)
Coupled Fe and S isotope variations in pyrite nodules from

references

Archean shale. Earth and Planetary Science Letters, 392, 67–79.

Marin-Carbonne J., Rollion-Bard C. and Luais B. (2011)
In-situ measurements of iron isotopes by SIMS: MC-ICP-MS intercalibration and application to a magnetite crystal from the Gunflint chert. Chemical Geology, 285, 50–61.

Nishizawa M., Yamamoto H., Ueno Y., Tsuruoka S., Shibuya T., Sawaki Y., Yamamoto S., Kon Y., Kitajima K., Komiya T., Maruyama S. and Hirata T. (2010)
Grain-scale iron isotopic distribution of pyrite from Precambrian shallow marine carbonate revealed by a femtosecond laser ablation multicollector ICP-MS technique: Possible proxy for the redox state of ancient seawater. Geochimica et Cosmochimica Acta, 74, 2760–2778.

Rudnick R.L. and Gao S. (2003)
Composition of the continental crust. Treatise on Geochemistry, 3, 1–64.

Virtasalo J.J., Laitala J.J., Lahtinen R. and Whitehouse M.J. (2015)
Pyritic event beds and sulfidized Fe (oxyhydr)oxide aggregates in metalliferous black mudstones of the Paleoproterozoic Talvivaara formation, Finland. Earth and Planetary Science Letters, 432, 449–460.

Virtasalo J.J., Whitehouse M.J. and Kotilainen A.T. (2013)
Iron isotope heterogeneity in pyrite fillings of Holocene worm burrows. Geology, 41, 39–42.

Weber T.S. and Deutsch C. (2010)
Ocean nutrient ratios governed by plankton biogeography. Nature, 467, 550–554.

Whitehouse M.J. and Fedo C.M. (2007)
Microscale heterogeneity of Fe isotopes in > 3.71 Ga banded iron formation from the Isua Greenstone Belt, Southwest Greenland. Geology, 35, 719–722.

Xie L.-W., Xu L., Yin Q.-Z., Yang Y.-H., Huang C. and Yang J.-H. (2018)
A novel sample cell for reducing the "Position Effect" in laser ablation MC-ICP-MS isotopic measurements. Journal of Analytical Atomic Spectrometry, 33, 1571–1578.

Xing C.C., Wang R.M., Shen B., Li C., Lang X.G. and Huang K.J. (2022)
The spatial distribution of surface ocean primary productivity in the wake of Marinoan global glaciation. Global and Planetary Change, 212, 103816.

Xu L., Xie LW., Wang H., Yang Y.H., Huang C., Yang J.H. and Wu S.T. (2022)
Evaluation of plasma condition, concentration effect, position effect, and nickel-doping method on non-matrix-matched Fe isotopic analysis by femtosecond laser ablation multi-collector inductively coupled plasma-mass spectrometry. Spectrochimica Acta Part B, 189, 106374.

Yoshiya K., Nishizawa M., Sawaki Y., Ueno Y., Komiya T., Yamada K., Yoshida N., Hirata T., Wada H. and Maruyama S. (2012)
In situ iron isotope analyses of pyrite and organic carbon isotope ratios in the Fortescue Group: Metabolic variations of a Late Archean ecosystem. Precambrian Research, 212, 169–193.

Yoshiya K., Sawaki Y., Hirata T., Maruyama S. and Komiya T. (2015a)
In-situ iron isotope analysis of pyrites in similar to 3.7 Ga sedimentary protoliths from the Isua supracrustal belt, southern West Greenland. Chemical Geology, 401, 126–139.

Yoshiya K., Sawaki Y., Shibuya T., Yamamoto S., Komiya T., Hirata T. and Maruyama S. (2015b)
In-situ iron isotope analyses of pyrites from 3.5 to 3.2 Ga sedimentary rocks of the Barberton Greenstone Belt, Kaapvaal Craton. Chemical Geology, 403, 58–73.

Zhang H.C., Zhu Y.F., Salvi S., Wu Y.F. and Gilbert S. (2022a)
Complex fluid source of the multistage pyrite-bearing Huilvshan gold deposit (west Junggar, NW China): Insight from pyrite texture, sulfur isotope and trace element compositions. Ore Geology Reviews, 149, 105081.

Zhang Y.W., Fan H.R., Santosh M., Xie LW., Hu F.F., Liu X., Hu H.L. and Li X.H. (2022b)
Iron and sulfur isotope fractionation during pyrite dissolution-reprecipitation revealed by in-situ isotopic analyses in the Muping gold deposit (Jiaodong, China). Journal of Asian Earth Sciences, 230, 105217.

Zheng X.Y., Beard B.L. and Johnson C.M. (2018)
Assessment of matrix effects associated with Fe isotope analysis using 266 nm femtosecond and 193 nm nanosecond laser ablation multi-collector inductively coupled plasma-mass spectrometry. Journal of Analytical Atomic Spectrometry, 33, 68–83.